Journal of Catalysis **208,** 150–157 (2002)
doi:10.1006/jcat.2002.3543, available online at http://www.idealibrary.com on IDEAL®

Synthesis, Characterization, and Catalytic Use of Acicular Iron Particles

Kenneth J. Takeuchi,*,[1] Amy C. Marschilok,* Carol A. Bessel,†,[1] and Norman R. Dollahon‡

*Department of Chemistry, State University of New York at Buffalo, Buffalo, New York 14260; and †Department of Chemistry, and ‡Department of Biology, Villanova University, 800 Lancaster Ave., Villanova, Pennsylvania 19085

Received October 2, 2001; revised January 17, 2002; accepted January 17, 2002

The synthesis of granular iron particles via hydrotriorganoborate reduction of $FeCl_3$ has been reported previously by several research groups. Notably, during the course of studying some of the reaction parameters involved in $FeCl_3$ reduction, we discovered the experimental conditions necessary to synthesize acicular iron particles, at low temperature and low pressure, in the absence of a constraining medium. Specifically, the effects of the reaction temperature, the stirring rate, and the $FeCl_3$ solution dropping rate on the size and morphology of the iron particles were examined. Under optimal conditions acicular iron particles were produced having diameters of ~300 nm, lengths on the order of tens to hundreds of micrometers, and surface areas of approximately 20 m^2/g. Both the acicular and the granular iron particles were found to be active catalysts for the formation of carbon nanofibers from the reaction of carbon monoxide and hydrogen gases. The graphitic natures of the carbon nanofibers formed from either acicular or granular iron catalysts were characterized by HRTEM and XRD. Also, while both types of iron catalysts produced straight carbon nanofiber morphologies, the granular iron catalysts also formed carbon nanofibers with spiral gross morphologies. Finally, the diameters of the carbon nanofibers were comparable to the diameters of the acicular or granular iron catalysts.

Key Words: **acicular iron particles; granular iron particles; carbon nanofibers.**

1. INTRODUCTION

The preparation of submicrometer-sized metal particles has been the topic of much recent research in areas as diverse as catalysis (1, 2), powder technology (3–5), nanoelectronics (6–9), and environmental chemistry (10). In particular, finely divided metal particles containing iron are of interest due to their use as catalysts in the preparation of an important family of carbon solids, namely, carbon nanofibers (*vide infra*) (11–16). Since the composition and the morphology of the metal catalysts can affect the structure of the carbon nanofibers, the study of novel forms of iron particles as catalysts may yield interesting carbon products.

[1] To whom correspondence should be addressed. For KJT: Fax: (716) 645-6963. E-mail: takeuchi@nsm.buffalo.edu; For CAB: Fax: (610) 519-7167. E-mail: carol.bessel@villanova.edu.

Two extremes in the morphology of finely divided iron powders are the granular and the acicular forms. Granular particles are approximately spherical in shape with an aspect ratio (length/width) near 1. Granular powders of iron, as well as a number of other metals, bimetallics, and metal alloys, have been generated from the hydrotriorganoborate reduction of a metal salt solution. These reactions generally proceed according to the following equation (written for iron)(2, 17):

$$FeCl_3 + 3LiBEt_3H \rightarrow Fe_{(s)} + 3LiCl + 3/2H_2 + 3BEt_3. \quad [1]$$

In this technique, a metal salt solution is gradually mixed with the reductant to precipitate a finely divided, granular metallic powder under low pressures and temperatures. Notably, acicular iron particles have not produced via the chemistry described in Eq. [1].

Acicular or fibrous particles are rodlike in nature, with a length significantly greater than their cross-sectional area (5). The synthesis of acicular iron particles generally requires additional synthetic considerations, such as the use of acicular starting materials, high pressures, high temperatures, constraining media, or magnetic fields (18–24). For examples of various synthetic strategies for the generation of acicular iron particles, consider the following reports. The use of acicular starting materials was investigated by Naono and also by Boennemann. Naono and co-workers reported the synthesis of acicular iron particles via reduction of silica-coated acicular hematite particles in air to form acicular iron products ~110 nm in length, with a surface area of 80 m^2/g and an aspect ratio of 10 (18). Boennemann *et al.* suspended acicular α-FeOOH particles in organic solvents and then chemically reduced the particles with a combination of hydrotriorganoborates and H_2 (20–100 bar) at 80°C to yield acicular iron products ~20 nm in diameter and 250 nm long (aspect ratio ca. 13) (17). The synthesis of acicular iron particles in constraining media was demonstrated by Nikles and co-workers in several reports (19–23). First, lecithin-encapsulated ferromagnetic α-iron particles were generated from a sodium borohydride reduction of ferrous chloride solutions containing soybean lecithin in the presence of an applied magnetic field (19–22). This preparation yielded acicular iron products that were

0021-9517/02 $35.00

0.25–5 micrometers in length with an aspect ratio of 6. In a separate report, ellipsoid-shaped β-FeOOH particles which had been prepared from the "forced hydrolysis" of ferric chloride were suspended in a lamellar liquid crystal phase and then reduced in a sodium borohydride solution. The resulting acicular iron products had aspect ratios greater than 5 and consisted of "chains of cubes," 20–25 nm in size (23). The use of magnetic fields for the formation of acicular iron particles was studied by Gedanken and co-workers (24). Acicular iron particles, 50 nm long and 5 nm wide, were synthesized via the sonochemical irradiation of a $Fe(CO)_5$ solution in decalin in the presence of a 7-kG external magnetic field. Iron products produced using similar reaction conditions in the absence of a magnetic field were found to be granular in nature, with a mean particle size of about 25 nm.

As mentioned above, the formation of nanostructured carbon materials from the interaction of metal catalyst particles with carbon-containing gases remains a subject of much interest, since carbon particles, fibers, and tubes have potential uses in electron emission devices (25–27), nanodevices (28, 29), hydrogen storage materials (30, 31), and fuel cells (1), as well as in other applications (15, 32). Rodriguez, Baker, and co-workers (11–13, 15) reported the formation of carbon nanofibers of various structures by controlling the nature of the metal catalyst surface, the composition of the reactant gases, the reaction temperature, and the presence of gas-phase or solid additives. The interaction of an iron-based catalyst with a 4 : 1 CO/H_2 mixture at 600°C resulted in a generation of carbon nanofibers having a "platelet" morphology consisting of graphite layers stacked parallel to the base of the metal catalyst and perpendicular to the fiber axis. The spacing between adjacent graphite layers compared well with that of single crystal graphite (0.335 nm). Generally, it has been noted that the diameters of carbon nanofibers are typically dictated by the size of the catalyst particle, with metal powder catalysts producing 5- to 500-nm diameter carbon fibers (15).

We report here the specific reaction conditions necessary to produce either granular or acicular iron particles via the hydrotriorganoborate reduction of $FeCl_3$. In particular, we discovered the experimental conditions which produce acicular iron particles with unusually large aspect ratios (>50). Notably, our synthetic method affords a low-temperature, low-pressure synthesis of acicular iron that does not require either acicular starting materials or a constraining medium. Also, using modifications to literature procedures (12), we report here the use of our acicular and granular iron particles as catalysts for the formation of carbon nanofibers from the reaction of carbon monoxide with hydrogen gas. The carbon nanofiber samples formed from the iron catalysts were characterized using BET, HRTEM, EDS, and XRD analyses.

2. EXPERIMENTAL AND METHODS

2.1. Materials

The syntheses and isolation of iron particles were carried out under inert atmospheres of nitrogen or argon. Iron trichloride (98%, assay) was purchased from Alfa AESAR. Lithium triethylhydridoborate, 1.0 M in tetrahydrofuran (THF), was purchased from Aldrich Chemical Company. Ethanol was purchased from Pharmco and distilled before use. Ultralow water tetrahydrofuran was purchased from JT Baker and used as received. Argon (99.998%), helium (99.995%), nitrogen (99.998%), and hydrogen (99.95%) were purchased from Irish Welding, and ultrahigh purity (UHP) carbon monoxide was purchased from Matheson Gas. All of the gases were used as received, except the nitrogen was purified before use by passage through a 500-cm^3 scrubbing column containing a 1 : 1 Ridox oxygen scavenging agent (Fisher Scientific Co.) and 13X molecular sieves (Davidson Chemicals).

2.2. Equipment

Kontes constant addition dropping funnels were used to achieve constant rates of addition of the $FeCl_3$ solution to the reductant solution. VWR Series 400S magnetic stirrers and VWR Spinplus stir bars were used to maintain constant and controlled stirring rates throughout the course of the reaction. The reaction temperature was held constant throughout the reaction using a Haake A80 constant temperature bath. A Thermolyne type F79300 tube furnace was used for preparation of carbon nanofiber samples.

A Hitachi S-570 scanning electron microscope was used for scanning electron microscopy (SEM) analysis. An accelerating voltage of 15 keV and a working distance of 25 mm were used. SEM samples were prepared on carbon adhesive tabs (Electron Microscopy Sciences). Scanning electron micrographs were taken with Polaroid Polar Pan 400 film. EDS was performed using a PGT IMIX-XD X-ray analysis system equipped with PGT IMIX microanalysis software, Version 8. The detector was a PGT Omega X-ray detector fitted with a barium light element window. The EDS samples were also prepared on carbon adhesive tabs. A JEOL JEM 2010 electron microscope was used for transmission electron microscopy (TEM) and high resolution transmission electron microscopy (HRTEM). TEM and HRTEM samples were mounted onto 300-mesh copper grids with a lacy SiO on Formvar support film (Ted Pella, Inc.). Surface area analyses were performed with an automatic volumetric sorption analyzer (Quantachrome NOVA 1200 Version 3.5 surface area analyzer) using N_2 as an adsorbate at −196°C. The surface areas were determined from the Brunauer–Emmett–Teller (BET) equation.

2.3. Synthesis of Iron Particles

Using modifications to a synthesis reported by Hampden-Smith and co-workers (2), 0.580 g (3.58 mmol) of $FeCl_3$ was stirred in 75 ml of THF for 8 h and then allowed to age without stirring for at least 48 h to allow complete formation of a red insoluble solid. The resulting pale yellow solution was filtered and then placed in a constant addition dropping funnel. These steps were performed in an inert atmosphere glove box. The $FeCl_3$ solution was then added dropwise to a stirring solution of 12 mL $LiBEt_3H$ in THF (1.0 M) and held at a constant temperature under an inert N_2 atmosphere. Returning to the glove box, the resulting black solid was separated from the reaction solution by vacuum filtration, washed first with 10 mL of a 1 : 1 mixture of THF/EtOH and then with 15 mL of THF, and finally dried *in vacuo*. Typical yields were ~90%, based on the initial $FeCl_3$ masses. The reaction conditions, which were carefully controlled and investigated, include (i) the dropping rate of the $FeCl_3$ solution, (ii) the stirring rate of the solution of 1.0 M $LiBEt_3H$ in THF, and (iii) the temperature of the reaction vessel containing the solution of 1.0 M $LiBEt_3H$ in THF.

2.4. Preparation of Carbon Nanofibers Catalyzed by Iron Particles

The iron particles were tested for their catalytic activity toward carbon formation using modifications of procedures previously reported by Rodriguez *et al.* (12). In an inert atmosphere glovebox, 6 mg of iron was weighed into a porcelain combustion boat which was then placed in the center of a quartz reaction tube. The reaction tube was sealed and then transferred from the glove box to a horizontal tube furnace, and the tube was purged for several minutes under a flow of helium gas. A 10% H_2/He mixture was introduced into the reaction tube as the oven was heated from room temperature of 600°C at a rate of 20°C/min. Following this heating and reduction step, a 4 : 1 CO/H_2 mixture was introduced into the reaction tube and carbon was formed for 6 h at a constant temperature of 600°C. Finally, the carbon produced was cooled to room temperature under He flow and passivated for 45 min using a 2% CO/He mixture before the carbon was removed from the reaction tube. In typical preparations, ~1.3 g of carbon was produced from 6 mg of iron catalyst.

2.5. Characterization of Iron Particles and Carbon Nanofibers

In an inert atmosphere glovebox, iron samples were prepared for SEM and EDS analyses by sprinkling the iron onto one side of double-sided sticky carbon tape (the other side adhered to an aluminum stub) and sealing the stubs in a capped vial. The vials were opened under a nitrogen gas flow, and the stubs were transferred quickly into the SEM sample chamber to minimize oxidation of the samples. (Caution: some of the iron samples were found to be pyrophoric.) Carbon nanofiber samples were also prepared on double-sided sticky carbon tape, but the stubs were not prepared or transferred under an inert atmosphere. Iron samples for BET analyses were weighed into glass cells in an inert atmosphere glovebox and then removed from the glovebox and inserted quickly into the BET instrument to minimize oxidation of the sample. Carbon samples were not transferred to the BET analyzer under an inert atmosphere. The iron samples were analyzed immediately, while the carbon nanofiber samples were vacuum outgassed for 2 h at 125°C prior to analysis. Selected iron and carbon samples were also studied using TEM and HRTEM. Iron samples were prepared by dispersing <1 mg of the iron in approximately 1 ml of dry ethanol and allowing two drops of this suspension to dry on the TEM grid in an inert atmosphere glovebox. Carbon samples were prepared by sonicating <1 mg of the carbon sample in approximately 1 ml *tert*-butanol and then the allowing 1 or 2 drops of this suspension to air-dry on the TEM grids.

In preparation for x-ray powder diffraction (XRD) analysis, our carbon nanofibers were stirred in 1 M hydrochloric acid solution for at least 2 days, then washed thoroughly with water, and finally dried under vacuum at 60°C. XRD data were collected with a Shimadzu Lab X-6000 X-ray diffractometer using Cu$K\alpha$ radiation. The carbon nanofiber samples were placed in an aluminum "well holder" with a sample chamber 25 mm in diameter × 1-mm deep. Fixed divergence and scatter slits of 1.00° and a receiving slit of 0.30 mm were used. The spacing between adjacent carbon layers (d_{002}) was determined using the Bragg equation, while the dimensions of crystallites with graphite-like order (L_{002}, L_{101}, L_{100}, L_{110}) were calculated using the Scherrer equation ($L = K\lambda/B\cos\vartheta$) and the values of the (002), (101), (100), and (110) reflections, respectively. For the 002 reflection, $K = 0.89$, while for the 101, 100, and 110 reflections, $K = 1.84$ was used (33).

3. RESULTS AND DISCUSSION

3.1. Iron Nanoparticle Synthesis and Characterization

In the course of preparing iron particles using reaction conditions described previously by Hampden-Smith and co-workers (2) and Bonnemann *et al.* (17), we found that the morphologies of the iron particles varied as a function of several reaction conditions, namely, the dropping rate of the $FeCl_3$/THF solution, the stir rate of the 1.0 M $LiBEt_3H$ in THF, and the reaction temperature. To quantitatively control the dropping rate, we employed a constant addition dropping funnel (Kontes). Also, a specialty magnetic stirrer (VWR series 400S) and a stir bar (VWR Spinplus) were required to control the stir rate of the reaction solution from 200 to 1600 rpm. Finally, the reaction temperature was controlled with a constant temperature bath.

First, a study was conducted to determine the effect of the $FeCl_3$/THF solution addition rate on iron particle morphology. Three experiments were conducted at a constant temperature (0°C) and at a constant stirring rate (200 rpm) of the $LiBEt_3H$ solution, where the addition rates of the $FeCl_3$/THF solution were 1 drop/10 s, 1 drop/s, or 2 drops/s. The low and high dropping rates were the minimum and maximum rates which the dropping funnel could maintain.

At the fastest addition rate (2 drops/s), the morphologies of the resulting iron particles were mixed. Some acicular and dendritic materials were present, but granular material was the primary product. The predominant granular particles had diameters of approximately 200–300 nm and specific surface areas of ca. 46 m^2/g. Simple geometric calculations based on the measured BET surface areas suggested that the granular iron particles might be agglomerates of smaller primary particles, with diameters of approximately 1–2 nm (assuming spherical primary particles with smooth, nonporous surfaces). This is consistent with the assertion by Hampden-Smith and co-workers that, based on BET measurements, 200-nm iron samples produced from the lithium triethylhydridoborate reduction of iron trichloride could be agglomerates of 2–4 nm primary particles (2). At the slowest addition rate (1 drop/10 s), the large majority of the product had an acicular morphology. The acicular particles had diameters of ~200 nm, lengths on the order of tens to hundreds of micrometers, and a specific surface area of ca. 17 m^2/g. Notably, our acicular iron particles display the *highest* aspect ratios ever reported (18–24).

From simple geometric considerations, spherical samples should display a larger surface area than that of acicular samples, given that both samples have approximately the same diameters and similar smooth, nonporous surfaces. This trend was observed within our addition rate experiments; specific surface areas ranged from 17 m^2/g at an addition rate of 1 drop/10 s (primarily acicular) to 46 m^2/g at an addition rate of 2 drops/s (primarily granular). Finally, the synthesis involving the intermediate dropping rate (1 drop/s) showed a distribution of granular and acicular iron particles between the distributions discussed above, reinforcing the above relationship between the slow addition rate and the high percentage of acicular iron products.

A second study was conducted to determine the effect of the stirring rate of the $LiBEt_3H$ solution on iron particle morphology. While a constant temperature of the $LiBEt_3H$ solution (0°C) and a constant addition rate of the $FeCl_3$ solution (1 drop/10 s), were maintained, three stirring rates of the $LiBEt_3H$ solution were employed: 200, 400, and 1600 rpm. The low and high values were chosen because they represented the minimum and maximum stirring rates which the magnetic stirrer and stir bar could maintain throughout the course of the reaction. At the highest stirring rate (1600 rpm), the iron particles that were formed were almost exclusively granular, with little to no acicular character. These granular particles had diameters of ~200–300 nm and specific surface areas of ~40 m^2/g (see Fig. 1). Simple geometric calculations (assuming spherical, smooth, nonporous primary particles) based on the measured BET (N_2) surface areas suggested that our granular iron particles might be agglomerates of smaller particles (*vide supra*). At the lowest stirring rate (200 rpm), the resulting iron particles were primarily acicular, with little to no granular character.

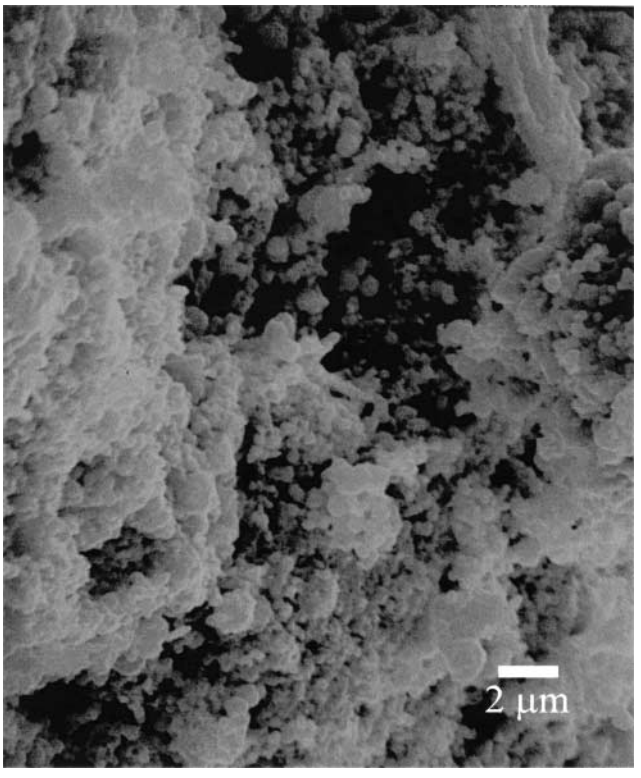

FIG. 1. SEM micrograph of iron particles (predominantly granular) formed at a reaction temperature of 0°C, a $FeCl_3$ solution addition rate of 0.1 drop/s, and a $LiBEt_3H$ solution stirring rate of 1600 rpm.

Specific surface areas ranged from 17 m^2/g at 200 rpm (primarily acicular) to 40 m^2/g at 1600 rpm (primarily granular), which is consistent with the surface area measurements for the dropping rate experiments (*vide supra*). Finally, the synthesis involving the intermediate stirring rate (400 rpm) showed a distribution of granular and acicular iron particles between the distributions discussed above, reinforcing the above relationship between the slow stirring rate and the high percentage of acicular iron products.

The final study on iron synthesis parameters was conducted to determine the effect of temperature on iron particle morphology. At a constant stirring rate of the $LiBEt_3H$ solution (200 rpm) and at a constant addition rate of the $FeCl_3$/THF solution (0.1 drop/s), the temperature of the $LiBEt_3H$ reaction solution was varied from 0 to 60°C. As anticipated from the selected stirring rate and addition

rate experiments, all iron particles formed in the temperature study were highly acicular. At lower temperatures (0–20°C), the iron products formed were almost exclusively single strands. At higher temperatures (40°C), the acicular strands became thinner and showed evidence of increased branching. The iron product formed at 60°C had a highly branched or weblike character. Specific surface areas in this series ranged from 17 m^2/g at 0°C to 42 m^2/g at 40°C. As a result of this study, it was determined that 20°C was an optimal temperature for the formation of single-stranded, acicular iron products.

Notably, our optimized acicular iron particles have unusual dimensions (see Fig. 2). Previously reported acicular iron particles display lengths of 10–100 μm and diameters of ∼200–300 nm, with aspect ratios ranging from ∼ 5 to ∼12 (18–24). Our iron particles have aspect ratios ranging from ∼50 to ∼500, which represent a notable increase in aspect ratios from those previously reported in the literature. Also, since HRTEM images of our acicular iron samples do not show individual spheres or cubes within a single acicular iron fiber (see Fig. 3), we propose that our acicular iron samples do not display a "chain of cubes" (23) morphology.

Finally, electron diffraction analysis of our highly acicular and highly granular iron samples showed both samples to be microcrystalline, with several phases of iron present, although it was not possible to conclusively identify each phase. Energy dispersive spectral analyses (EDS) showed the samples to be homogeneous, with iron as the only element detected.

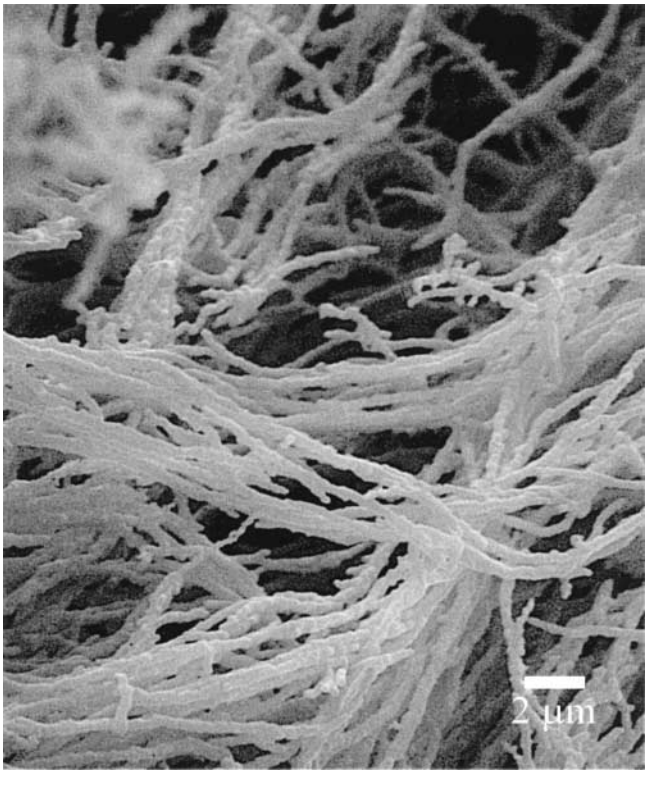

FIG. 2. SEM micrograph of iron particles (predominantly acicular) formed at a reaction temperature of 20°C, a $FeCl_3$ solution addition rate of 0.1 drop/s, and a $LiBEt_3H$ solution stirring rate of 200 rpm.

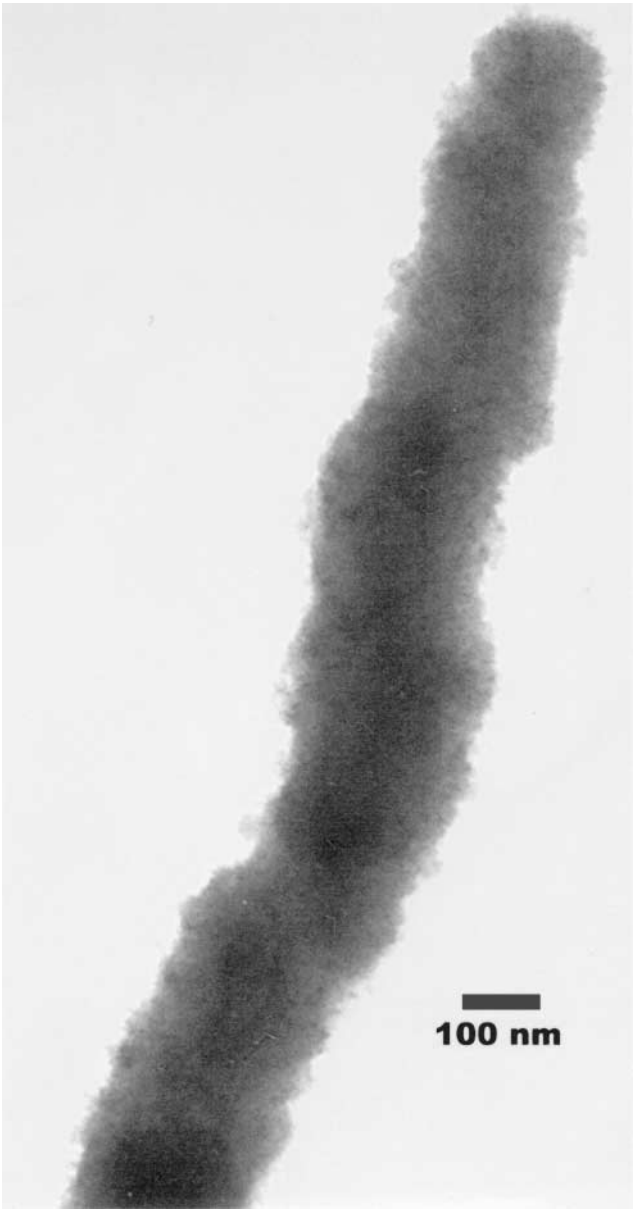

FIG. 3. HRTEM micrograph of an individual acicular iron particle from the collection of iron particles shown in Fig. 2.

3.2. Carbon Nanofiber Preparation and Characterization

Carbon nanofibers were synthesized using our acicular or granular iron particles as catalysts, in a modification of a procedure previously reported by Rodriguez *et al.* (12). In typical preparations, ∼1.3 g of carbon was produced from 6 mg of iron catalyst after 6 h of carbon deposition. BET surface area analyses showed that the carbon samples

produced from granular and acicular iron catalysts had specific surface areas of ca. 130 and 160 m^2/g, respectively. EDS of the carbon samples produced from granular and acicular iron catalysts were similar, showing large peaks for carbon and small peaks corresponding to the residual catalyst on exposure to air (i.e., iron and oxygen) which were just above the level of the background noise.

The carbon nanofiber samples were imaged using SEM, TEM, and HRTEM. For the carbon fibers prepared from either granular or acicular iron catalysts, the catalyst particle was typically observed at one end of the fiber. No evidence was seen for the existence of branched fibers from either sample. Carbon nanofibers produced from either acicular or granular iron catalysts showed similar fine structures under high magnification, namely, regions of ordered graphitic planes along the edges of the fibers (see HRTEM image, Fig. 4). Additionally, the spacings between the graphitic planes in the carbon nanofibers were found to be ~0.34 nm, reminiscent of the spacings found in single-crystal graphite.

XRD analysis was used to gain information about the dimensions of the ordered regions in the two types of carbon nanofiber samples. The spacing between adjacent carbon layers d_{002} was found to be similar, with carbon nanofibers produced from acicular and granular iron catalysts having spacings of 3.40 and 3.41 Å, respectively. The dimensions of the parallel carbon layers ($L_{101}, L_{100}, L_{110}$) were determined from the (101), (100), and (110) reflections, respectively, and the average stacking height of parallel layers (L_{002}) was determined from the (002) reflection. The carbon nanofibers produced from acicular iron catalysts had an L_{002} of 57 Å, an L_{101} of 162 Å, an L_{110} of 211 Å, and an L_{100} of 92 Å. Interestingly, the carbon nanofibers produced from granular iron catalysts had larger dimensions, with an L_{002} of 72 Å, an L_{101} of 270 Å, an L_{110} of 290 Å, and an L_{100} of 100 Å. This result suggests that the morphology of the iron catalyst does have an effect on crystallite dimensions of the resulting carbon nanofibers.

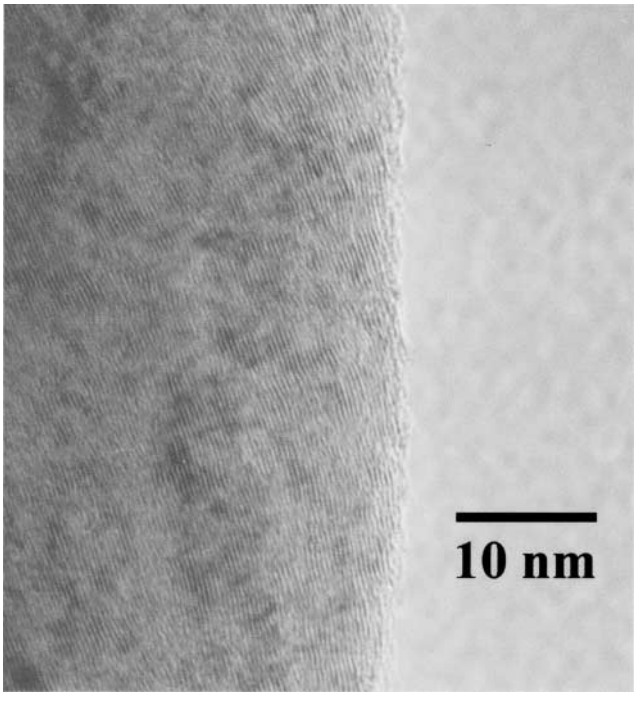

FIG. 4. HRTEM micrograph showing graphitic platelets of an individual carbon nanofiber from the collection of carbon nanofibers shown in Fig. 6.

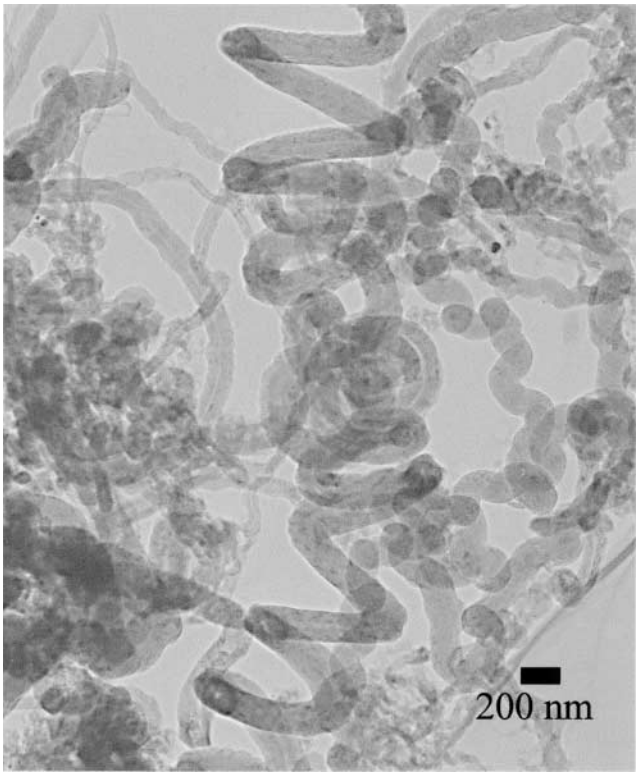

FIG. 5. TEM micrograph of carbon nanofibers grown from the granular iron catalyst shown in Fig. 1.

Interestingly, some of the carbon nanofibers grown from the granular iron catalyst displayed a spiral gross morphology under lower magnification (see TEM image, Fig. 5). This morphology was not observed in the carbon grown from the acicular iron catalyst, where the carbon nanofibers were straight or gently curved (see TEM image, Fig. 6). It has been previously shown that the symmetrical diffusion of the carbonaceous starting materials through the metal catalysts results in the generation of relatively straight fibers, while unsymmetrical diffusion results in the generation of twisted or helical fibers. It has also been noted that the presence of additives in the metal particle can promote formation of these twisted structures, as they may alter the diffusion pathway of the catalyst (34–38). Our results indicate that the morphology of the iron catalyst may be a third influence on the structure of the carbon nanofibers.

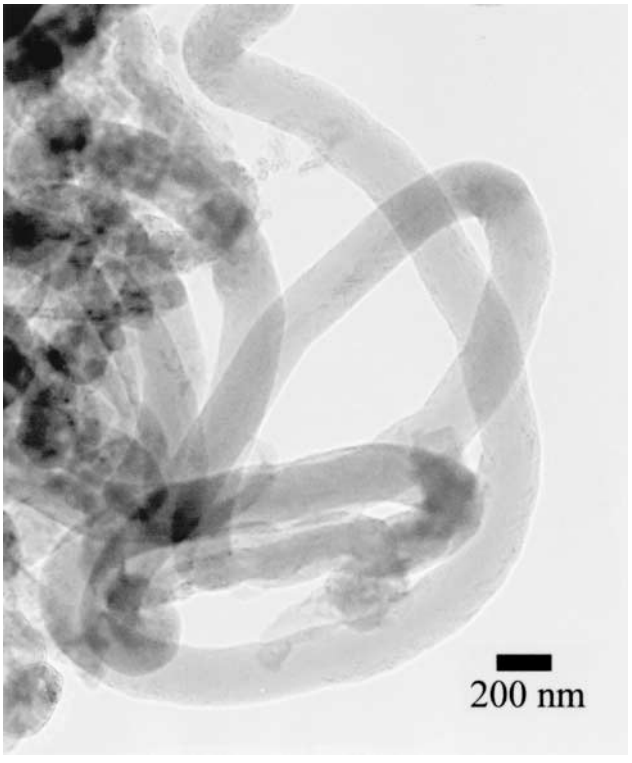

FIG. 6. TEM micrograph of carbon nanofibers grown from the acicular iron catalyst shown in Figs. 2 and 3.

Finally, while the granular iron catalyst particles were structurally robust under carbon fiber formation conditions, some fragmentation did occur with the acicular catalyst particles. Analysis of the electron micrographs indicates that the acicular particles undergo transverse fragmentation to form more granular particles of a diameter similar to that of the starting acicular particles, but of aspect ratios closer to 1. Other authors have noted that fragmentation of the powdered metal starting materials is possible during the carbon deposition process and that the diameter of the active metal catalyst may be smaller than the diameter of the powdered metal starting materials (15). As a result, the diameter of the carbon nanofiber can be smaller than the diameter of the powdered metal starting material. However, in our observation, the cross-sectional diameter of the carbon nanofibers matched the diameter of the powdered metal starting materials from which they were produced, suggesting that the diameter of our active metal catalysts matches the diameter of our powdered metal starting materials. The diameters of the starting acicular and granular iron powders were similar, on the order of 200–300 nm, and the diameters of the carbon nanofibers formed from both powders were also similar, approximately 200–300 nm. In carbon nanofiber micrographs in which intact metal catalysts were visible, the catalyst particle was typically at one end of the nanofiber.

4. CONCLUSIONS

With precise control of key reaction conditions, it is possible to utilize a single-step chemical reduction method to produce iron particles that are either primarily acicular or granular in morphology. The acicular iron particles formed herein are notable in that their aspect ratios are unusually large (50–500). Both the acicular and the granular iron particles functioned well as catalysts for carbon nanofiber formation. The carbon nanofibers were found to be at least partially graphitic in nature, and the d_{002} spacings were very similar, but the crystallite dimensions differed, depending on whether the iron catalyst was acicular or granular. In addition, the diameters of the iron catalysts corresponded to the diameters of the carbon nanofibers, and the formation of carbon nanofibers having a straight or spiral gross morphology may be related in part to the iron catalyst morphology. Thus, future studies are warranted, where further modification of either the iron catalyst structure or the composition may provide some tuning of the graphitic properties and the gross morphologies of carbon nanofibers and ultimately some control of their chemical properties.

ACKNOWLEDGMENTS

This work was supported in part by grants from the Research Corporation (ROA for KJT, and CC4252 for CAB) and from the Office of Naval Research (N00014-96-1-0047 for CAB).

REFERENCES

1. Bessel, C. A., Laubernds, N. M., Rodriguez, N. M., and Baker, R. T. K., *J. Phys. Chem. B* **105**(6), 1115 (2001).
2. Duan, Z., Hampden-Smith, M. J., Datye, A., Nigrey, P., Quintana, C., and Sylwester, A. P., *J. Catal.* **139**, 504 (1993).
3. Kieffer, R., and Benesovsky, F., *Ullmanns Encykl. Tech. Chem.* **4**, 563 (1980).
4. Roll, K. H., *Kirk-Othmer Encycl. Chem. Tech*. **3**, 28 (1982).
5. Lee, P. W., Trudel, Y., Iacocca, R., German, R. M., Ferguson, B. L., Eisen, W. B., Moyer, K., Madan, D., and Sanderow, H., Eds., "ASM Handbook, Vol 7: Powder Metal Technologies and Applications," ASM International, Materials Park, OH, 1998.
6. Rao, C. N. R., Kulkarni, G. U., Govindaraj, A., Satishkumar, B. C., and John Thomas, P., *Pure Appl. Chem.* **72**(1–2), 21 (2000).
7. Fendler, J. H., Ed., "Nanoparticles and Nanostructured Films." Wiley–VCH, Weinheim, 1998.
8. Braunstein, P., Oro, G., and Raithby, P. R., Eds., "Metal Clusters in Chemistry, Nanomaterials and Solid State Chemistry," Vol. 3. Wiley–VCH, Weinheim, 1999.
9. Markovich, G., Collier, C. P., Henrichs, S. E., Remacle, F., Levine, R. D., and Heath, J. R., *Acc. Chem. Res.* **32**, 397 (1999).
10. For recent examples of environmental chemistry involving iron particles, see (a) Farrell, J., Melitas, N, Kason, M., and Li, T., *Environ. Sci. Technol.* **34**, 2549 (2001); (b) Schuetz, C., Winther, K., and Kjeldsen, P., *Environ. Sci. Technol.* **34**, 2557 (2001); (c) Ponder, S. M., Darab, J. G., and Mallouk, T. E., *Environ. Sci. Technol.* **34**, 2564 (2001).
11. Baker, R. T. K., *Carbon* **27**, 315 (1989).

12. Rodriguez, N. M., Chambers, A., and Baker, R. T. K., *Langmuir* **11**, 3862 (1995).
13. Baker, R. T. K., and Rodriguez, N. M., *in* Catalytic growth of carbon nanofibers and nanotubes. "Novel Forms of Carbon II." Vol. 349, pp. 251–256. Materials Research Society, Pittsburgh, PA, 1994.
14. Hernadi, K., Fonseca, A., Nagy, J. B., Bernaerts, D., and Lucas, A. A., *Carbon* **34**(10), 1249 (1996).
15. Rodriguez, N. M., *J. Mater. Res*. **8**, 3233 (1993) and references therein.
16. Yang, R. T., and Chen, J. P., *J. Catal.* **115**, 52 (1989).
17. Boennemann, H., Brijoux, W., Brinkmann, R., Fretzen, R., Joussen, T., Koeppler, R., Korall, B., Neitler, P., and Richter, J., *J. Mol. Catal.* **86**, 129 (1994).
18. Sueyoshi, T., Naono, H., and Amemiya, M., *IEEE Trans. Magn*. **23**, 80 (1987).
19. Cain, J. L., and Nikles, D. E., *J. Appl. Phys.* **79**, 4860 (1996).
20. Cain, J. L., and Nikles, D. E., *IEEE Trans. Magn.* **32**, 4490 (1996).
21. Cain, J. L., and Nikles, D. E., *IEEE Trans. Magn.* **33**, 3718 (1997).
22. Chen, M., and Nikles, D. E., *J. Appl. Phys.* **85**, 5504 (1999).
23. Chen, M., Tang, B., and Nikles, D. E., *IEEE Trans. Magn.* **34**, 1141 (1998).
24. Prozorov, T., Prozorov, R., Koltypin, Y., Felner, I., and Gedanken, A., *J. Phys. Chem. B* **102**, 10,165 (1998).
25. de Heer, W. A., Chatelain, A., and Ugarte, D., *Science.* **270**, 1179 (1995).
26. Rinzler, A. G., Hafner, J. H., Nikolaev, P., Lou, L., Kim, S. G., Tomanek, D., Nordlander, P., Colbert, D. T., and Smalley, R. E., *Science* **269**, 1550 (1995).
27. Wang, Q. H., Setlur, A. A., Laverhaas, J. M., Dai, J. Y., Seelig, E. W., and Chang, R. P. H., *Appl. Phys. Lett.* **272**, 2912 (1998).
28. Collins, P. G., Zettl, A., Bando, H., Thess, A., and Smalley, R. E., *Science* **278**, 100 (1997).
29. Frank, S., Poncharal, P., Wang, Z. L., and de Heer, W. A., *Science* **280**, 1744 (1998).
30. Chambers, A., Park, C., Baker, R. T. K., and Rodriguez, N. M., *J. Phys. Chem. B* **102**, 4253 (1998).
31. Park, C., Anderson, P. E., Chambers, A., Tan, C. D., Hidalgo, R., and Rodriguez, N. M., *J. Phys. Chem. B* **103**, 10,572 (1999).
32. Ebbesen, T. W., "Carbon Nanotubes: Preparation and Properties." CRC Press, Boca Raton, FL, 1997.
33. Kinoshita, Kim, "Carbon: Electrochemical and Physicochemical Properties." Wiley, New York, 1988.
34. Anderson, P. E., and Rodriguez, N. M., *Chem. Mater.* **12**, 823 (2000).
35. Nishiyama, Y., and Tamai, Y., *J. Catal.* **33**, 98 (1974).
36. De Bokx, P. K., Kock, A. J. H. M., Boellaard, E., Klop, W., and Geus, J. W., *J. Catal.* **96**, 454 (1985).
37. Kim, M. S., Rodriguez, N. M., and Baker, R. T. K., *J. Catal.* **131**, 60 (1991).
38. Krishnankutty, N., Park, C., Rodriguez, N. M., and Baker, R. T. K., *Catal. Today* **37**, 295 (1997).